



A model to simulate the gravitropic response and internal stresses in trees, considering the progressive maturation of wood

Guillaume Pot, Catherine Coutand, Evelyne Toussaint, Jean-Benoit Le Cam,
M. Saudreau

► To cite this version:

Guillaume Pot, Catherine Coutand, Evelyne Toussaint, Jean-Benoit Le Cam, M. Saudreau. A model to simulate the gravitropic response and internal stresses in trees, considering the progressive maturation of wood. *Trees - Structure and Function*, 2014, 28 (4), pp.1235-1248. 10.1007/s00468-014-1033-y . hal-01063248

HAL Id: hal-01063248

<https://hal.science/hal-01063248>

Submitted on 17 Nov 2014

HAL is a multi-disciplinary open access archive for the deposit and dissemination of scientific research documents, whether they are published or not. The documents may come from teaching and research institutions in France or abroad, or from public or private research centers.

L'archive ouverte pluridisciplinaire **HAL**, est destinée au dépôt et à la diffusion de documents scientifiques de niveau recherche, publiés ou non, émanant des établissements d'enseignement et de recherche français ou étrangers, des laboratoires publics ou privés.

Copyright

A model to simulate the gravitropic response and internal stresses in trees, considering the progressive maturation of wood

Guillaume Pot · Catherine Coutand · Evelyne
Toussaint · Jean-Benoît Le Cam · Marc Saudreau

Received: date / Accepted: date

Key Message: The developed model of gravitropism takes non instantaneous maturation of wood into account which enabled to correctly simulate different gravitropic phases and realistic internal stress profiles.

Abstract A new biomechanical model of tree movement in relation to gravity (gravitropism) is proposed in this study. The modelling of the progressive maturation of wood cells is taken into account, as well as spatio-temporal variations in maturation strains (MS) and mechanical properties. MS were identified using an inverse method that allows the model to fit the gravitropic reaction observed experimentally. For this

This work was supported by a grant from the Auvergne Regional Council and the European Regional Development Fund.

G. Pot
LaBoMaP, Arts et Metiers ParisTech, Rue Porte de Paris, F-71250 Cluny, France
E-mail: guillaume.pot@ensam.eu

C. Coutand
INRA, UMR 547 PIAF, F-63100 Clermont-Ferrand, France
Clermont Université, Université Blaise Pascal, UMR 547 PIAF, F-63000 Clermont-Ferrand, France
E-mail: Catherine.Coutand@clermont.inra.fr

E. Toussaint
CNRS, UMR 6602, Institut Pascal, F-63171 Aubière, France
Clermont Université, Université Blaise Pascal, Institut Pascal, BP 10448 F-63000 Clermont-Ferrand, France
Tel.: +33473 40 53 81
Fax: +33473 40 74 94
E-mail: evelyne.toussaint@univ-bpclermont.fr

J.-B. Le Cam
UNIVERSITE DE RENNES 1, Institut de Physique de Rennes, UMR 6251, Campus de Beaulieu, 35042 Rennes, France
E-mail: jean-benoit.lecam@univ-rennes1.fr

M. Saudreau
INRA, UMR 547 PIAF, F-63100 Clermont-Ferrand, France
Clermont Université, Université Blaise Pascal, UMR 547 PIAF, F-63000 Clermont-Ferrand, France
E-mail: Marc.Saudreau@clermont.inra.fr

purpose, the curvature during righting movement, the geometry and the mass distribution of a two-year-old poplar tree were measured. The identified MS are higher than expected, which shows the underestimation of MS by usual measurements. By using the same mechanical parameters and MS as an input, the model gives satisfying results in terms of shape modelling for different trees up to 32 days after tree tilting. The model is able to simulate the latency phase observed in the tree righting movement, and the internal stress profile in the trunk is realistic (low compressive value in the central part of the trunk and zero stress in newly-formed cells). The next development of the model will aim to simulate the end of the gravitropic phase in relation with the regulation of MS by the tree.

Keywords Gravitropism · Biomechanical model · Poplar

Authors contributions to the paper:

G. Pot participated to model building, simulations analyses and writing of the paper.

C. Coutand participated to model building, simulations analyses and writing of the paper.

E. Toussaint participated to model building, simulations analyses and writing of the paper.

J.B. Le Cam participated to model building, simulations analyses and writing of the paper.

M. Saudreau participated to the optimization procedure for the identification of the parameters of the model.

1 Introduction

Trees can maintain or modify the orientation of their trunk or branches in relation to gravity. These gravitropic movements are enabled by the asymmetrical production of reaction wood in plant parts that have achieved their elongation (Scurfield, 1973). In most deciduous species, reaction wood is called tension wood (TW) because this wood is subjected to longitudinal tensile stresses within the living tree. Stresses in trees are mainly due to the wood cell maturation process. During their maturation, wood cells tend to shrink in their longitudinal direction, but these maturation strains (MS) are impeded by the cells created earlier, which are already stiffer, thus producing internal maturation stresses (Kubler, 1959). The high internal stresses caused by TW can induce damage during wood exploitation and processing (Cassens and Serrano, 2004).

At the beginning of the righting-up movement of a tilted trunk, deciduous trees create TW with high internal stresses on the upper face of the tilted trunk, and so-called opposite wood (OW) with low internal

stresses on the lower face (on the opposite side). In fact, a recent study on the kinematics of the gravitropic movement of artificially tilted poplars (Coutand et al, 2007) revealed three phases: a latency phase (no curving up of the tilted trunk), a gravitropic phase (curving up) and an autotropic phase (decurving enabling the trunk to become straight and vertical). Within this last phase TW is produced on the opposite side.

Several biomechanical models concerning tree gravitropism can be found in the literature. They were built to simulate the movement of growing trees and/or to compute the internal stresses with a technological aim (because of the splitting or twisting of planks due to stresses). Kubler (1959) was the first author to calculate analytically the internal stresses in the case of a trunk growing symmetrically for an elastic and transversally isotropic material. Then Archer and Byrnes (1974) extended these formulae for asymmetrical growth. Later, Fournier et al (1991a,b) developed a semi-analytical model which showed that maturation stresses are much greater than stresses due to the self-weight of the tree. Numerical finite element modelling of tree shape regulation was also developed by Fourcaud et al (2003). Recently, biomechanical models have shown that viscoelasticity can increase the righting-up efficiency of trees (Dlouhá et al, 2008; Coutand et al, 2011). These biomechanical models consider that the maturation process is instantaneous: when cells are created in the model, they immediately acquire the mechanical properties of a matured wood cell and they produce a given level of MS.

As noticed by Coutand et al (2007), gravitropic righting in young poplar trees occurs over a few weeks; thus the kinetics of maturation (*i.e.* changes with time in terms of mechanical properties and MS) could have an effect on the gravitropic response. Nevertheless, none of the existing biomechanical models considers a progressive maturation. Moreover, they do not usually use experimentally determined properties as input data, and thus cannot be compared to experimental measurements of gravitropic movement.

In the present paper, a model is built with the aim of simulating the righting-up of tilted trees which create TW on the upper face of the trunk during a single season of growth. Both progressive maturation and the viscoelasticity of green wood are taken into account. The objectives are (i) to compare the proposed model featuring progressive maturation to models with instantaneous maturation and (ii) to compare the model to experimental measurements to estimate MS by inverse identification.

After the present introduction, the second part of this work presents the biomechanical model, with special emphasis on the modelling of progressive maturation. In the third part, the experimental data used as the input to the model and the identification of MS are presented. Then the results are discussed and

conclusions are drawn concerning the value of MS obtained and the ability of the model to simulate tree gravitropism.

2 Biomechanical modelling

2.1 General description of the model

The biomechanical model presented in the following is an enhancement of the model of Coutand et al (2011) (TWIG). As in this previous work, it is programmed using MATLAB version 7.5 (2007). The same principles of modelling are used, typically the geometrical definition of the tree and the incremental formulation of the viscoelastic behaviour. They are briefly recalled hereafter.

The TWIG model (Coutand et al, 2011) is a semi-analytical model based on Euler-Bernoulli beam theory. The mechanical properties used are those of wood in the longitudinal direction. According to Fournier et al (1991b), such a model is sufficient to approach the longitudinal internal stresses that are the main cause of tree gravitropic movements.

The tree is modelled by a beam whose diameter evolves discontinuously along its length L in n_{seg} cylindrical segments, themselves numbered i_{seg} (Fig. 1a, b). This model does not account for the longitudinal growth. Indeed, experimental measurements show that longitudinal growth is small during gravitropic reaction (Pot, 2012). However, it could be modelled using an additional mass at the tip of the beam.

Asymmetrical radial growth is modelled considering the eccentricity of the outer cylinder of each segment relatively to the pith (Fig. 1). The coefficient δ is the distance between the centre of the pith and the centre of the new outer cylinder. The difference in mechanical properties between TW and OW is taken into account thanks to the division of the cross section of the beam into two angular sectors, defined by angle γ (Fig. 1c, d). Model parameters depend on the face considered and are named using the index "up" for parameters relative to the upper face of the tilted tree and "low" for parameters relative to the lower face of the tilted tree. For the sake of simplicity, the "face" index is used in the following as a generic term for "up" or "low".

The beam in Fig. 1a is anchored at its base and the external forces are only due to the self-weight of the structure. Branches are not represented, but their effect in terms of weight is considered as a distributed mass which can evolve during the growing season (see section 3.3 for details). Weight induces a normal force

N^w , a shear force T^w and a bending moment M^w on the structure. Shear forces are neglected, in keeping with the Euler-Bernoulli assumption. Maturation induces internal normal forces N^m and bending moments M^m which bend the beam. Finally, the total normal forces and bending moments are noted in a vector $\{F\}$ as the sum of the normal forces and bending moments due to weight and maturation:

$$\{F\} = \begin{Bmatrix} N^w + N^m \\ M^w + M^m \end{Bmatrix}_{Oxyz} \quad (1)$$

These normal forces and bending moments produce a longitudinal strain along the axis that is noted ε_O and a curvature (χ) of the beam. It is also noted in vector form (named the vector of generalised strains) as follows:

$$\{D\} = \begin{Bmatrix} \varepsilon_O \\ \chi \end{Bmatrix}_{Oxyz} \quad (2)$$

2.2 Spatio-temporal description

In order to model the maturation process, the variations over time of wood mechanical properties must be taken into account. Since the tree is growing in diameter, there are also spatial variations in the whole structure. This is the reason why it is necessary to consider the spatio-temporal variation of the parameters. In the model, radial growth is considered as an incremental problem: growth is modelled by the addition at each time step i_t of a new radial growth increment $i_{dr} = i_t$ (Fig. 1). By this means, every radial growth increment is denoted at every time step using index i_{dr} . This enables the spatial heterogeneity of the beam to be represented.

The duration of growth that is simulated, denoted T , is divided into n growth increments. Thus, the duration of a growth increment is $\Delta t_{dr} = \frac{T}{n}$. Thanks to the distinction between spatial and temporal increments, it is possible to define the time at the beginning of the current growth step as:

$$t(i_t) = i_t \Delta t_{dr} \quad (3)$$

and the time of creation of a given growth increment i_{dr} as:

$$t(i_{dr}) = i_{dr} \Delta t_{dr} \quad (4)$$

With these two characteristic times, it is possible to define the age of each growth increment, denoted \hat{a} . The age of a growth increment is defined as the difference between the time at the end of the current growth step and the time of creation of the increment. Thus, the age of a given growth increment at time step i_t is:

$$\hat{a} = (i_t + 1 - i_{dr})\Delta t_{dr} \quad (5)$$

By this means, when a growth increment is created at a given time step, it immediately has an age of Δt_{dr} .

This age has a physical meaning, since it corresponds to the age of the wood cells contained in the modelled tree. It enables the modelling of the change in mechanical properties according to the maturation stage of each increment.

Finally, any parameter P of the model depends on spatial and temporal increments, and can be written as $P_{face}(i_{seg}, i_{dr}, i_t)$. It varies with the circumferential position ("face" index), the longitudinal position (i_{seg}), the radial position (i_{dr}), and the time (i_t). The decoupling between spatial and temporal increments enables the parameters of each spatial increment to vary freely with time increments. This decoupling is the main contribution of the present work, since other models usually consider instantaneous maturation for which the parameters of spatial increments do not change with time after their creation.

2.3 Incremental formulation of viscoelastic behaviour

As in Coutand et al (2011), a viscoelastic constitutive law of green wood mechanical behaviour and an incremental calculation method are used to model tree gravitropism. The fundamental principle of this modelling is to decompose time into increments of Δt and calculate Boltzmann's equation over the finite time interval $[t, t + \Delta t]$, under the hypothesis of linearity over this interval. This leads to the following equation:

$$\{\Delta F\} = [K^*] \{\Delta D\} + \{F^{hist}\} \quad (6)$$

where $\{\Delta F\}$ is the variation in normal force and bending moment during time increment Δt ; $[K^*]$ is the fictitious stiffness matrix; $\{\Delta D\}$ is the variation in longitudinal strain and curvature during time increment Δt ; and $\{F^{hist}\}$ is the normal force and bending moment which accounts for the effect of the total load history since the beginning of the loading period.

The viscoelastic constitutive law used is based on a Burgers' rheological model (Fig. 2), in accordance with the results of Pot et al (2013b). By this means, Burgers' rheological parameters appear in mathematical expressions of $[K^*]$ and $\{F^{hist}\}$ (Pot, 2012), but the fundamental principle of incremental formulation do not change with respect to Jurkiewicz et al (1999) or Coutand et al (2011).

The time increments of the viscoelastic calculation (Δt) are different from time increments that describe the growth of the trunk (denoted Δt_{dr}). Indeed, the time increments of the incremental viscoelastic formulation must be short enough to observe the hypothesis of the linearity of the equations (Jurkiewicz et al, 1999). The duration of growth increments cannot be short enough to verify linearity, because it would lead to a high number of spatial increment and thus high dimensions for matrix and vectors, which would overload memory. Consequently, growth time increments are subdivided into viscoelastic calculation time increments. Thus, the calculation is divided into two steps:

1. The first calculation is performed at the beginning of each growth step, thus at time $t(i_t)$. The variation in force and moment due to maturation and weight are then calculated and equation 6 is solved.
2. Next, a calculation loop is performed without considering growth and maturation. However tree movements and changes in internal forces can appear because of viscoelasticity and weight. Time t is incremented in the viscoelastic formulation with the short time increment Δt until the next growth increment.

During these two calculation steps, the viscoelastic formulation (equation 6) is inverted and used for each segment in order to obtain the variation in generalised strains $\{\Delta D(i_{seg}, t)\}$:

$$\{\Delta D(i_{seg}, t)\} = [K^*(i_{seg}, t)]^{-1} \left(\{\Delta F(i_{seg}, t)\} - \{F^{hist}(i_{seg}, t)\} \right) \quad (7)$$

The same formulation is used for steps where growth and maturation appear and steps where only the effect of viscoelasticity is concerned. However, when growth occurs, maturation forces appear in $\{\Delta F(i_{seg}, t)\}$ and the mechanical parameters are changed.

2.4 Determination of time step size and computational errors

2.4.1 Influence of time step size on viscoelastic calculation

The influence of time step size on viscoelastic calculation was determined thanks to a preliminary study on the creep of a wood beam. This beam had similar characteristics as those used in the present study. A 3

m long cylindrical homogeneous beam of radius $r = 15$ mm and density of $\rho = 500 \text{ kg.m}^{-3}$ was tilted to $\alpha = 35^\circ$ from the vertical and its deflection under self-weight was modeled. The analytical expression of the curvature can be easily calculated in the case of a non-growing beam:

$$\chi(x, t) = J(t) \frac{M^w(x)}{I(x)} \quad (8)$$

with $J(t) = \frac{1}{E_0} + \frac{t}{E_0 \tau_\infty} + \frac{1}{E_1} (1 - e^{-t/\tau_1})$ the compliance function of Burgers' model (with notations of Fig. 2), I the second moment of inertia, and $M^w(x)$ the bending moment along the position x in the stem due to self weight. Burgers model parameters are mean value find in Pot et al (2013b): $E_0 = 3$ GPa, $E_1 = 3.5$ GPa, $\tau_1 = 38$ hours, and $\tau_\infty = 200$ days.

The evolution with time of curvature at stem base obtained with the model is presented in Fig. 3a for different sizes of time step (Δt), and compared to the analytical result. The less the Δt , the more the accuracy of the model. With the lowest time step size presented here, $\Delta t = 0.0063$ days (9 minutes), the maximum relative error between model and theoretical formula is 0.17%.

2.4.2 Influence of growth step size

The discretization of the viscoelastic calculation is not the only source of computational error: the quantity of growth increments may have an influence on the accuracy of the computation because of the decoupling between growth and mechanical effect (see Guillon et al (2012) for more details about the numerical methods for the biomechanics of growing trees). However, there are no analytical results for a viscoelastic growing beam, thus no comparison with the model can be completed. A simple way to evaluate the effect of growth increment size is to compare the results obtained for different quantity of growth increments.

The temporal evolution of the curvature at trunk base during radial growth and gravitropic reaction has been compared to computation with 10, 50, 111 and 1 110 growth increments, each of them being divided in 100 viscoelastic increments. Here, the input data of the model are those defined in part 3 for tree A, that is the same input data as those used for discussing the results in part 4. The results presented in Fig. 3b show that curves obtained for 50, 111 and 1 110 growth increments are superimposed. Between the 111 and 1 110 growth increments calculations, the relative difference in curvature is about 0.82%.

This low difference allows us to ignore computational errors concerning the comparison between model results and experimental measurements of curvature. Moreover, in all following calculations, 111 growth

increments (Δt_{dr}) divided in 100 viscoelastic increments (Δt) will be used during the calculation period of 70 days. This quantity of growth increments corresponds to the limit of a classical 32-bit operating system because of the maximum memory size of 2 GB allocated to MATLAB on such systems.

2.5 Modelling normal forces and bending moments due to maturation

In equation 7, the variation in normal forces and bending moments $\{\Delta F(i_{seg}, t)\}$ is calculated as the sum of the normal forces and bending moments due to weight and maturation (see equation 1).

Normal forces and bending moments due to weight can easily be calculated using knowledge of wood density and radial growth increments. Thus, the variation is calculated as the difference between two time steps.

Normal forces and bending moments due to maturation are calculated by considering that maturation stresses are generated at the time of the creation of growth increments by the full locking of MS. Thanks to the model presented above, these MS can vary with each spatial or growth temporal increment; they are denoted $\Delta \varepsilon_{face}^m(i_{seg}, i_{dr}, t(i_t))$. The maturation stresses created because of the impediment of these MS are calculated thanks to the modulus of elasticity (MOE) of Burgers' model, denoted $E_{0,face}(i_{seg}, i_{dr}, i_t)$, as follows:

$$\Delta \sigma_{face}^m(i_{seg}, i_{dr}, t(i_t)) = E_{0,face}(i_{seg}, i_{dr}, t(i_t)) \Delta \varepsilon_{face}^m(i_{seg}, i_{dr}, t(i_t)) \quad (9)$$

Normal forces ΔN^m and bending moments ΔM^m produced by these maturation stresses are calculated by integration onto the surface of each spatial increment denoted $S_{face}(i_{seg}, i_{dr})$:

$$\begin{cases} \Delta N_{face}^m(i_{seg}, i_{dr}, t(i_t)) = \int_{S_{face}(i_{seg}, i_{dr})} \Delta \sigma_{face}^m(i_{seg}, i_{dr}, t(i_t)) dS \\ \Delta M_{face}^m(i_{seg}, i_{dr}, t(i_t)) = \int_{S_{face}(i_{seg}, i_{dr})} \Delta \sigma_{face}^m(i_{seg}, i_{dr}, t(i_t)) z dS \end{cases} \quad (10)$$

Since MOE and MS are constant within a single spatial increment, normal forces and bending moments due to wood maturation can be written as follows:

$$\begin{cases} \Delta N_{face}^m(i_{seg}, i_{dr}, t(i_t)) = E_{0,face}(i_{seg}, i_{dr}, t(i_t)) \Delta \varepsilon_{face}^m(i_{seg}, i_{dr}, t(i_t)) S_{face}(i_{seg}, i_{dr}) \\ \Delta M_{face}^m(i_{seg}, i_{dr}, t(i_t)) = E_{0,face}(i_{seg}, i_{dr}, t(i_t)) \Delta \varepsilon_{face}^m(i_{seg}, i_{dr}, t(i_t)) A_{face}(i_{seg}, i_{dr}) \end{cases} \quad (11)$$

where $A_{face}(i_{seg}, i_{dr}) = \int_{S_{face}(i_{seg}, i_{dr})} z dS$ is the static moment of a given spatial increment. The total increments of normal forces and bending moments due to wood maturation on a given segment and time increment are computed as the sum of the normal forces and bending moments on each radial increment of the upper and lower face. This gives finally:

$$\begin{cases} \Delta N^m(i_{seg}, t(i_t)) = \sum_{i_{dr}=1}^{i_{dr}=i_t} \Delta N_{sup}^m(i_{seg}, i_{dr}, t(i_t)) + \Delta N_{inf}^m(i_{seg}, i_{dr}, t(i_t)) \\ \Delta M^m(i_{seg}, t(i_t)) = \sum_{i_{dr}=1}^{i_{dr}=i_t} \Delta M_{sup}^m(i_{seg}, i_{dr}, t(i_t)) + \Delta M_{inf}^m(i_{seg}, i_{dr}, t(i_t)) \end{cases} \quad (12)$$

3 Input data of the model

The model described above is able to consider any spatio-temporal variations in mechanical parameters. Input data are needed for this model: spatio-temporal variation in geometry, mass, viscoelastic properties, and MS must be known. Several prior experimental studies (Coutand et al, 2007; Pot et al, 2013a,b; Pot, 2012) are used to this end. However, it is not possible to measure MS variations during wood maturation. Since the variations of the other parameters were known, MS were obtained by inverse identification thanks to the comparison between tree righting calculated with the model and the experimental observations. The MS temporal variation obtained from this identification is presented in this section, as well as input parameters that were measured experimentally (mechanical properties, cross section geometry and mass distribution). The principal input parameters of the model with progressive maturation are summarized in table 2.

The experimental data are measured on two different sets of two-year-old hybrid poplars (*Populus deltoides* x *Populus nigra*, cv I4551) that were tilted by about 35° from the vertical at the beginning of the growing season. A first set of seven trees was used in Pot (2012) and Pot et al (2013b) to measure mechanical properties and mass distribution during 63 days. A second set of four trees was used specifically for the present work for cross section and shape measurement in order to perform a comparison between the experimental and modelled righting of trees during gravitropic reaction. They were felled at the end of the season. They are named A, B, C and D in the following.

3.1 Mechanical properties

Pot et al (2013b) performed creep tests on wood samples harvested in the basal part of the trunk. They give temporal variations in the parameters of Burgers' model according to the age of the wood cells. In this study, it is assumed that all cells have the same viscoelastic properties once they are matured. This approximation is consistent with the results of Pot et al (2013a). In addition, negligible differences were found by Pot et al (2013b) between the viscoelastic behaviour of OW and that of TW.

Consequently, in the present model, the same values of viscoelastic parameters are used for both faces. Without any information about longitudinal variations, it is assumed that mechanical properties do not vary with the longitudinal position in the tree. For the sake of simplicity, longitudinal increments i_{seg} and "face" index are omitted in expressions of viscoelastic parameters. Finally, viscoelastic parameters depend only on the maturation state, *i.e.* wood cell age. In the model, the relation between age and radial increments i_{dr} or temporal increments i_t is obtained thanks to equation 5.

Temporal variations in each viscoelastic parameter of Burgers' model are approximated by appropriate mathematical functions that smooth the variations of the experimental data (see Fig. 9 in Pot et al (2013b)). Thus, E_1 is modelled by a linear function: $E_1(\hat{a}) = 1.1 + 0.17\hat{a}$ where E_1 is in GPa and \hat{a} in days. η_1 is obtained by the relation $\eta_1 = E_1\tau_1$ with a constant value of $\tau_1 = 38$ hours. $\frac{1}{\eta_\infty}$ is modelled by a slightly decreasing exponential function: $\frac{1}{\eta_\infty} = 6.75 \cdot 10^{-12} \exp(-9.4 \cdot 10^{-3}\hat{a})$, where η_∞ is in Pa.days and \hat{a} in days.

The temporal variation of E_0 was studied in Pot (2012). It was modelled thanks to the addition of an exponential function and a Gaussian function that are schematically presented in Fig. 4. Contrary to other parameters of Burger's model, it was shown that there is a difference between TW and OW: the height of the peak due to the Gaussian function was higher for TW (6500 MPa) than for OW (3800 MPa).

3.2 Cross section geometry

The diameter of trees A, B, C and D was regularly measured during the season from the base to the top of the tree as described in Coutand et al (2007); Pot (2012). The diameter at the trunk base on the day of tilting is presented in table 1. The spatial and temporal variations in diameter for each of these trees are used as input data in the biomechanical model.

The cross section is supposed to be perfectly circular. The geometry is defined thanks to the eccentricity of the growth increments and a TW sector angle (Fig. 1). Eccentricity is defined by a coefficient of eccentricity set to 0.4, which means that the centre of each growth increment is located at a distance from the pith centre of 40% of the growth ring thickness. This value was found in Pot et al (2013b). The angle of the TW sector is set to 180° thanks to experimental measurements which show that it does not significantly vary with longitudinal position in the tree and that the mean value is $180 \pm 20^\circ$ (Pot, 2012). As a first approximation, both of these geometrical parameters are considered constant with space and time.

The pith is considered in the cross section as a cylinder of constant radius of $r_{pith} = 2.65$ mm, according to experimental measurements all along the trunk (Pot, 2012). Note that pith is considered as an elastic material with a MOE of 30 MPa, which is one hundred-fold lower than wood, as suggested by Alm  ras and Fournier (2009).

3.3 Mass distribution

3.3.1 Mass distribution along the trunk

The mass distribution of the two sets of trees (11 trees) was measured by weighing different parts of the trees. After tree felling, the trunk was divided into logs of 35 cm length. They were weighed when the trees were felled (*i.e.* in green state). Density was then calculated thanks to diameter measurements under the hypothesis of a perfectly conical shape. The results for trees felled at different dates along the season are shown in Fig. 5a. It appears that green wood density increases from about 600 to 1100 kg.m^{-3} along the length of the trunk. This result could be due to a higher water content in the upper parts of the trunk. Indeed, the pith is in greater proportion in the upper part of the trunk since its diameter remains almost constant along the tree. This highly porous material must be full of water and then have a density close to 1000 kg.m^{-3} , which finally induces a higher density at the top of the tree.

In the following, the longitudinal variation in wood density is modelled thanks to a cubic polynomial equation that fits the experimental data, as follows:

$$\rho(x) = 17.42x^3 - 0.91x^2 - 3.25x + 627.50 \quad (13)$$

where ρ is the density in kg.m^{-3} and x is the distance from trunk base in m. Since the density is used in the model, the mass of the trunk automatically increases when growth occurs.

3.3.2 Mass distribution of the foliage

The mass of the foliage of the set of seven trees felled at different dates along the season is presented in Fig. 5b. It appears that there is an increase in foliage mass along the season. A linear approximation gives a rate of mass increase of $3.6 \cdot 10^{-3} \text{ kg.day}^{-1}$. This rate was used to model the temporal variation in foliage mass of each tree.

The mass of the foliage of trees A, B, C and D was measured at the end of the season. The foliage was divided in two parts along the trunk, and the length of these parts was measured. The total mass for each tree is presented in table 1. Note that foliage mass can vary by 30% between trees. In the model, the foliage mass of each tree is used in input by distributing linearly the mass of the two measured parts over their length for each tree. The variation in foliage mass along the season is modelled thanks to the rate of mass increase found above. It is important to take this variation into account, because over a period of 70 days the foliage mass can vary by more than 50%. In terms of mass it represents about 40% of the total tree mass.

3.4 Maturation strains

3.4.1 Definition of the temporal variation

To the best of the authors knowledge, no method for measuring MS during wood maturation exists, whereas it is the most influential parameter according to various authors (Alméras et al, 2005; Coutand et al, 2011). Measurements of residual longitudinal maturation strains (RLMS) exist, but they give information on strains in the periphery of the tree only, *i.e.* cells that are always in the same maturation state. As mentioned by Gril and Thibaut (1994), MS must not appear instantaneously; therefore it is necessary to consider their temporal variation with maturation (wood cell age in our case). Moreover, the level of MS produced by wood cells may vary along the season and with the gravitropic response because of different qualities of TW, as mentioned by Coutand et al (2007). Thus, it seems necessary to model temporal variations in terms of MS that are due both to maturation and variations along the season.

A Gaussian cumulative distribution function was chosen to model the temporal variation in MS with wood cell age (Fig. 6a). The shape of such a function enables the modelling of a smooth increase in MS during a customizable period (the maturation time), and then an asymptote is reached, which models the half of MS creation when the wood cells are mature. MS variation with wood cell age for a given face is defined by the equation:

$$\varepsilon_{face}^m(\hat{a}, t) = \varepsilon_{tot, face}^m(t) \int_0^{\hat{a}} \exp\left(\frac{(u - \tau_{\hat{a}, face})^2 \ln(0.01)}{(\delta_{\hat{a}, face}/2)^2}\right) du \quad (14)$$

where $\tau_{\hat{a}, face}$ is the characteristic time which defines the middle of the distribution, $\delta_{\hat{a}, face}$ is the width of the distribution at 1% of its height, and $\varepsilon_{tot}^m(t)$ is the final value of MS when the total strain has been reached.

$\varepsilon_{tot}^m(t)$ can vary with time in order to model variations in MS along the season. Its variations are arbitrarily defined with the same type of Gaussian distribution function (Fig. 6b):

$$\varepsilon_{tot, face}^m(t) = C_{face} \int_0^t \exp\left(\frac{(u - \tau_{t, face})^2 \ln(0.01)}{(\delta_{t, face}/2)^2}\right) du \quad (15)$$

where $\tau_{t, face}$ is the characteristic time which define the middle of the distribution, $\delta_{t, face}$ is the width of the distribution at 1% of its height, and C_{face} is a constant which is adjusted in order to obtain the desired maximum value of MS (which is noted $\varepsilon_{tot, face}^m(t \mapsto +\infty)$). With this second function, wood cells created at the beginning of the gravitropic reaction produce lower MS than wood cells created later in the season, which simulates a variation in TW quality at the beginning of the gravitropic reaction. This function determines the regulation of MS along the season regardless of the righting of the tree, thus it must be identified from experimental measurements.

3.4.2 Inverse identification of MS temporal variation

Because of the lack of experimental methods to determine the MS temporal variations, the parameters defined above were identified by fitting the modelled temporal variations of the curvature at the trunk base of tree A to experimental data. To identify model parameters, some assumptions were made, because the numerous parameters induce an indeterminate system. Firstly, the same temporal parameters were used for both upper and lower faces, which means that maturation was presumed to occur at the same rate in both

TW and OW. Secondly, the temporal parameters relative to MS variations with wood cell age were fixed according to experimental data:

- $\delta_{\hat{a},face}$, which is the duration of maturation in terms of MS, is determined thanks to an experimental study (see Pot (2012)) which showed that the MOE increases while maturing up to 13 to 25 days after cell creation. In the present study, it is assumed that the average of this duration corresponds to the duration of the maturation in terms of MS, thus: $\delta_{\hat{a},face} = 19$ days.
- $\tau_{\hat{a},face}$, which is the time when MS reach 50% of their final value, can be reasonably bounded between 5 and 12 days. Indeed, higher value than 12 days would lead to very low deformations for wood cells aged of 8 days (cf. $\tau_{\hat{a},face} = 15$ days in Fig. 6a), which is not consistent with the fact that RLMS measurements provide significant deformations in the first millimeter of the outer part of growing trees (see Coutand et al (2014)). Lower value than 5 days would signify that maturation is almost instantaneous, this particular case is discussed in part 4.

Thirdly, the maximum MS of the lower face, denoted $\varepsilon_{tot,inf}^m(t \mapsto +\infty)$ was set to 0.005. By doing so, it represents a moderate proportion (between 11% and 36%) of the maximum MS of the upper face that is found below, which seems probable.

By considering these assumptions, the maximum MS of the upper face ($\varepsilon_{tot,sup}^m(t \mapsto +\infty)$) and the temporal parameters relative to its variation along the season ($\tau_{t,face}$ and $\delta_{t,face}$) were identified by minimizing the squared differences between experimental and modelled curvature at trunk base of tree A up to 32 days after tilting. The optimization was done thanks to a constrained interior-point algorithm. Lower and upper boundaries of the optimization were chosen to keep a physical meaning of the parameters, that is : $1 < \tau_{t,face} < 30$, $2 < \delta_{t,face} < 70$ and $0.005 < \varepsilon_{tot,sup}^m(t \mapsto +\infty) < 0.1$. Different initial values of the parameters were tested close to these bounds, without significant change in the optimized result.

Three different values of $\tau_{\hat{a},face}$ were tested in input (5, 8 and 12 days, cf. Fig. 6a). The results are presented in table 3. The identification gives an interval of $[0.014; 0.044]$ for $\varepsilon_{tot,sup}^m(t \mapsto +\infty)$, which is discussed in section 4.4. The three results are comparable in term of fitting of the temporal evolution of curvature. In the following discussions, the parameters obtained for $\tau_{\hat{a},face} = 8$ days are chosen. These parameters are listed in table 2. The corresponding MS temporal variation along the season is presented in Fig. 6b. Thanks to these parameters, the temporal variation in tree A curvature at the trunk base was

correctly simulated up to 32 days after tilting (Fig. 7a). The MS parameters obtained for this tree were then used to simulate the gravitropic reaction of trees B, C and D (see section 4.3).

3.5 Input data for the elastic model and the model with instantaneous maturation

The parameters used for the viscoelastic model with progressive maturation are described in the above sections. To the best knowledge of the authors, it is the first time that such a model has been proposed; it is useful, therefore, to compare it to models with more usual hypothesis. To do this, the same model was used but the input parameters were modified.

Firstly, the effect of viscoelasticity was studied in comparison with an elastic model with progressive maturation. The same MOE and MS parameters as viscoelastic with progressive maturation calculation were used. The only difference was the viscoelastic behaviour, which was not taken into account.

Secondly, the proposed model was compared to a classical elastic model with instantaneous maturation. MOE were set instantaneously to their mean value according to experimental bending tests, that is $E_{0,inf}(i_{seg}, i_{dr}, t) = 3$ GPa for the lower face and $E_{0,sup}(i_{seg}, i_{dr}, t) = 5.1$ GPa for the upper face. This induces better righting-up efficiency; thus, it was necessary to use lower MS to obtain the same curvature. This is why, by maintaining the same value of MS of 0.005 on the lower face, MS of 0.0052 on the upper face enabled us to obtain the same curvature value as with experimental measurements 28 days after tilting.

4 Results and discussion

4.1 Comparison of curvature

Results of the model in terms of curvature at the trunk base are presented in Fig. 7a. They are compared to experimental data (solid black line). Despite the better righting-up efficiency regarding the level of MS, an elastic model with instantaneous maturation (dash-dotted green line) cannot correctly simulate the temporal curvature variation. Indeed, the lag period during which there is no tree curvature cannot be simulated. For this instantaneous model, the curvature increases quickly at the beginning of growth, and then the rate of curvature decreases progressively because of the increase in diameter of the trunk. Indeed, this increase in diameter induces an increase in flexural rigidity, which counterbalances the effect of MS.

Conversely, the viscoelastic model with progressive maturation (solid red line) can simulate the slow decrease in curvature during the first days after tilting. This decrease is explained by the shape of the temporal variation in MS maximum value, increase in tree weight, and viscoelastic creep. The elastic calculation (dashed blue line) shows that the decrease in curvature is lower than that obtained with the viscoelastic model with progressive maturation in this zone. The quick increase in curvature between 18 and 32 days after tilting is also steeper with the viscoelastic model with progressive maturation than for the elastic model with progressive maturation. This shows that viscoelasticity has a significant effect on tree gravitropism, which was already highlighted by the models of Dlouhá et al (2008) and Coutand et al (2011). However, this is the first time to the authors knowledge that this result has been confirmed by using experimental data as an input to the model.

From 32 days after tilting to 70 days after tilting, the rate of curvature in the model remains almost constant, while experimental results show a decrease in this rate. The model's behaviour is consistent with the temporal variation in total MS used, which reaches its maximum value about 32 days after tilting (Fig. 6b) and then remains constant. To model the decrease in curvature rate that is observed experimentally, it would be necessary to change the temporal variation of MS along the season, with a decrease 32 days after tilting. This result shows that there is a decrease in the intensity of MS, which can be interpreted as the regulation of the level of MS by the tree in order to avoid becoming too curved and exceeding the vertical limit. This latter explanation is consistent with the results of Coutand et al (2007), which show that there exists an autotropic phase when the trunk is decurved to finally become straight and vertical.

4.2 Comparison of stress profiles

In Fig. 7b, the stress profiles of tree A obtained with the model for the same three assumptions discussed above are presented (no experimental data are available). The stress profiles are compared to the only temporal position when the curvature at the trunk base is almost the same for each model, that is 28 days after tilting. Consequently, these 3 different stress profiles give rise to the same trunk curvature.

All three models present a Kubler-like profile (Kubler, 1959) in the central part, with a radius of between 2.65 mm and 17.6 mm from the centre of the pith. This is due to the initial calculation of the model, for which the tree is considered to grow symmetrically with OW mechanical properties up to the radius measured

when tree was tilted, that is 17.6 mm for tree A. Stresses in the pith are not presented, since its MOE is very low.

It is worth noting that compressive stresses close to the pith reach very high negative values for the elastic model with instantaneous maturation (less than -80 MPa), whereas taking maturation into account leads to maximum compressive stresses of -40 MPa and adding viscoelasticity leads to maximum compressive stresses of -20 MPa. The results of the elastic model with instantaneous maturation are consistent with theoretical model of Kubler (1959), for which stresses tend towards infinity close to the pith. However, this result is not physically admissible, contrary to the stress profile obtained thanks to the proposed model, for which both progressive maturation and viscoelasticity induce lower compressive stresses.

A discontinuity in stresses is observed when the tree is tilted, corresponding to a radius of 17.6 mm in Fig. 7b. This is due to the inclination of the tree, which induces a brutal change in stresses. When the tree is tilted, the upper face is tensed and the lower face is compressed. Then new growth increments begin their maturation on a structure for which internal stresses have changed instantaneously, bringing about the observed discontinuity.

In the part of the tree that grows when the tree was tilted ($r > 17.6$ mm), the elastic model with instantaneous maturation presents a quasi-linear shape for the stress profile, while models with progressive maturation show a more complex profile. For the model with instantaneous maturation, stress is maximum at the periphery of the tree *i.e.* newly formed cells. This is not realistic, because cells that have just been created are not mature and have a very low MOE, thus they cannot exhibit such a stress level. Conversely, models with progressive maturation show zero stress for new cells, and it increases progressively as the cells become older, *i.e.* the distance from the periphery increases. This is due to the progressive appearance of both MS and MOE variations, which are defined in Fig. 4 and 6a. Moreover, stresses in the zone of 17.6 to 19 mm from the pith on the upper face of the tree are lower for models with progressive maturation than for models with instantaneous maturation. This is due to the progressive increase in total MS after tilting (Fig. 6b), which enables the lag period to fit the curvature.

4.3 Comparison of the shape of different trees

Fig. 8 presents both the modelled and experimental shapes of the 4 trees named A, B, C, D at different times after tilting. As explained before, the diameter and foliage mass of each tree were used as an input for

the model, but mechanical properties and MS are the same for all four trees. Trees B, C and D can differ from tree A by up to 31% in foliage mass and 14% in diameter at the trunk base (table 1). This difference in trunk diameter results in a difference in the second moment of area up to 68%. The second moment of area is proportional to flexural rigidity; thus the forces necessary to right-up these different trees are significantly different. Using the model with the same MS and mechanical parameters for these different trees enables us to test the robustness of the model.

The initial deflection just after tilting is well described for each tree all along its length (dashed-dotted blue lines in Fig. 8). This shows that MOE measurements by bending tests are appropriate to modelling tree mechanical behaviour, and that the hypothesis of a constant MOE all along the trunk is admissible before gravitropic reaction.

The modelled shape of tree A 28 days after tilting is compared with experimental measurements (dashed green lines in Fig. 8a). The modelled curvature fits the experimental data not only at the trunk base as shown in Fig. 7a, but also all along the trunk. This validates the hypothesis of identical maturation in terms of MS and MOE all along the trunk up to 28 days after tilting.

For trees B, C and D, experimental and modelled shapes 28 days after tilting are in good agreement. The same observation can be made 7 days after tilting, when the 4 trees present, experimentally and by modelling, a similar sagging. The same observations can be made for intermediate times. Thus, by using exactly the same mechanical properties and MS temporal variation, the model can simulate the gravitropic movement of different trees up to 28 days after tilting. However, from 28 to 32 days after tilting, the model and experimental results start to diverge, and finally the modelled shape 70 days after tilting is very different from the experimental shape, as shown for each tree of Fig. 7. This divergence appears while the temporal variation of total MS defined here remains constant over time (Fig. 5b). Thus, this behaviour shows that MS must start to decrease about 30 days after tilting, possibly because of an autotropic reaction that prevents the tree to overshoot the vertical. Indeed, in a recent paper (Coutand et al, 2014), it is shown that RLMS of the upper side start to decrease about 35 days after tilting.

4.4 Discussion on MS modelling

By using the same mechanical parameters and MS in input, the viscoelastic model with progressive maturation presents satisfying results in terms of shape modelling for different trees up to 32 days after tilting.

The maximum MS values of the upper face, which are obtained by inverse identification, are between 0.014 and 0.044 (with maximum MS of the lower face set to 0.005). These level of strain are far greater than the RLMS measurements of TW performed on the same tree clones (less than 0.003 in (Coutand et al, 2014)). However, such strains are necessary to obtain the high curvature increase between 18 and 32 days after tilting.

This discrepancy could be explained by the fact that RLMS are not a good indicator of the MS that exist in the tree. Indeed, RLMS measurements were performed on several wood cells located in the periphery of the trunk (see Yang and Waugh (2001) for a review). In the part of the tree where these measurements were performed, there are cells in different maturation states, and thus the RLMS are not representative of the MS of wood cells that are fully matured. Moreover, RLMS measurements are elastic measures: the deformation due to stress release is measured instantaneously just after the grooves are made. Thus, viscoelastic deformations do not have time to occur during the measurement, whereas the viscoelastic behaviour of wood is significant, as it was shown in a previous work (Pot et al, 2013b). Indeed, it was shown in this latter study that longitudinal slats of green TW that are harvested from poplar trees and maintained in water curve over a period of several weeks because of internal maturation stresses and the viscoelastic behaviour of green wood. This curvature reach a value of 0.019 mm^{-1} in average for slats that are in the periphery of the tree. Assuming that maturation stresses are fully released when this autonomous curvature is reached, the radius of curvature, *i.e.* wood deformations, are linked to the differential of MS between the two sides of the slat. With a curvature of 0.019 mm^{-1} and a thickness of 1.3 mm as in Pot et al (2013b), a value of 0.025 for this differential of MS between the two sides of the slat is obtained. Since these strains are only due to the release of internal stresses, this shows that wood cells can reach strains of the same order of magnitude as those found by inverse identification thanks to the present model. Consequently, it can be concluded that RLMS cannot be assimilated to the MS that really occur during wood cell maturation. It would be useful to establish a relationship between RLMS and MS. Finally, the assumption of the model concerning MS seems acceptable in order to model quantitatively the first steps of gravitropic reaction.

5 Conclusion

A biomechanical model of tree gravitropism is proposed in this work. The main contribution is the modelling of the progressive maturation of wood while the tree is growing. This is done by taking into account spatio-

temporal changes in the mechanical properties. The model uses experimental data of temporal and spatial variations in geometry and the mechanical properties of young poplar trees. To the best of the authors' knowledge, this is the first time that such comparisons between biomechanical model and experimental measurements of gravitropism have been performed.

MS were identified thanks to the model in order to fit the temporal variation in the curvature of a given tree during its gravitropic reaction. The testing of these MS on the gravitropic reaction of four different trees shows that the hypotheses made concerning temporal variations in MS are relevant. It appears that MS in TW must be higher than those obtained with usual estimations of MS, which are based on RLMS measurements. As a result, the exploitation of the present model shows that RLMS measurements underestimate the MS that are really experienced by wood cells. The main suspected cause is the viscoelastic behaviour of green wood, which is not taken into account by RLMS measurements.

The proposed model provides significant improvements in the modelling of tree gravitropism. Firstly, the modelling of temporal variations in MS over the course of the season enables the simulation of the temporal variation in tree curvature in the latency phase and at the beginning of the gravitropic phase. Secondly, the internal stress profile in the trunk is more realistic than stress profiles obtained with elastic models or models with instantaneous maturation. Further work is currently being carried out to simulate the end of the gravitropic phase (and possibly the autotropic phase) by taking into account the regulation of MS.

Conflict of interest: The authors declare that they have no conflict of interest.

References

- Alméras T, Fournier M (2009) Biomechanical design and long-term stability of trees: morphological and wood traits involved in the balance between weight increase and the gravitropic reaction. *J Theor Biol* 256:370–381, DOI 10.1016/j.jtbi.2008.10.011
- Alméras T, Thibaut A, Gril J (2005) Effect of circumferential heterogeneity of wood maturation strain, modulus of elasticity and radial growth on the regulation of stem orientation in trees. *Trees* 19:457–467, DOI 10.1007/s00468-005-0407-6
- Archer R, Byrnes F (1974) On the distribution of tree growth stresses. part i: An anisotropic plane strain theory. *Wood Sci Technol* 8:184–196, DOI 10.1007/BF00352022
- Cassens DL, Serrano JR (2004) Growth stress in hardwood timber. 14th Central Hardwood Forest conference, Wooster Ohio, DOI 10.1126/science.179.4074.647
- Coutand C, Fournier M, Moulia B (2007) The gravitropic response of poplar trunks: Key roles of pre-stressed wood regulation and the relative kinetics of cambial growth versus wood maturation. *Plant Physiol* 144:1166–1180
- Coutand C, Mathias JD, Jeronimidis G, Destrebecq JF (2011) Twig: A model to simulate the gravitropic response of a tree axis in the frame of elasticity and viscoelasticity, at intra-annual time scale. *J Theor Biol* 273:115–129, DOI 10.1016/j.jtbi.2010.12.027
- Coutand C, Pot G, Badel E (2014) Mechanosensing is involved in the regulation of autostress levels in tension wood. *Trees* pp 1–11, DOI 10.1007/s00468-014-0981-6
- Dlouhá J, Alméras T, Clair B, Gril J, Horacek P (2008) Biomechanical performances of trees in the phase of active reorientation. *Acta Univ Agric Silv Mendel Brun* 56:39–44
- Fourcaud T, Blaise F, Lac P, Castéra P, de Reffye P (2003) Numerical modelling of shape regulation and growth stresses in trees. *Trees* 17:31–39, DOI 10.1007/s00468-002-0203-5
- Fournier M, Chanson B, Thibaut B, Guitard D (1991a) Mechanics of standing trees: modelling a growing structure submitted to continuous and fluctuating loads. 1. analysis of support stresses. *Ann For Sci* 48:513–525, DOI 10.1051/forest:19910504

- Fournier M, Chanson B, Thibaut B, Guitard D (1991b) Mechanics of standing trees: modelling a growing structure submitted to continuous and fluctuating loads. 2. tridimensional analysis of maturation stresses. case of standard hardwood. *Ann For Sci* 48:527–546, DOI 10.1051/forest:19910504
- Gril J, Thibaut B (1994) Tree mechanics and wood mechanics: relating hygothermal recovery of green wood to the maturation process. *Ann For Sci* 51:329–338, DOI 10.1051/forest:19940311
- Guillon T, Dumont Y, Fourcaud T (2012) Numerical methods for the biomechanics of growing trees. *Comput Math Appl* 64:289–309
- Jurkiewicz B, Destrebecq JF, Vergne A (1999) Incremental analysis of time-dependent effects in composite structures. *Comput & Struct* 73:425–435, DOI 10.1016/S0045-7949(98)00269-7
- Kubler H (1959) Studies on growth stresses in trees. 1. the origin of growth stresses and the stresses in transverse direction. *Holz als Roh Werkstoff* 17:1–9
- MATLAB version 75 (2007) The MathWorks, Inc., Natick, Massachusetts, United States
- Pot G (2012) Mechanical characterization of green wood during maturation process and modeling of gravitropic reaction of young poplar. PhD thesis, Blaise Pascal University
- Pot G, Coutand C, Le Cam JB, Toussaint E (2013a) Experimental study of the mechanical behaviour of thin slices of maturing green poplar wood using cyclic tensile tests. *Wood Sci Technol* 47:7–25, DOI 10.1007/s00226-012-0477-8
- Pot G, Toussaint E, Coutand C, Le Cam JB (2013b) Experimental study of the viscoelastic properties of green poplar wood during maturation. *J Mat Sci* 48:6065–6073, DOI 10.1007/s10853-013-7403-9
- Scurfield G (1973) Reaction wood: Its structure and function. *Science* 179:647–655
- Yang JL, Waugh G (2001) Growth stress, its measurement and effects. *Austr Forest* 64:99–104

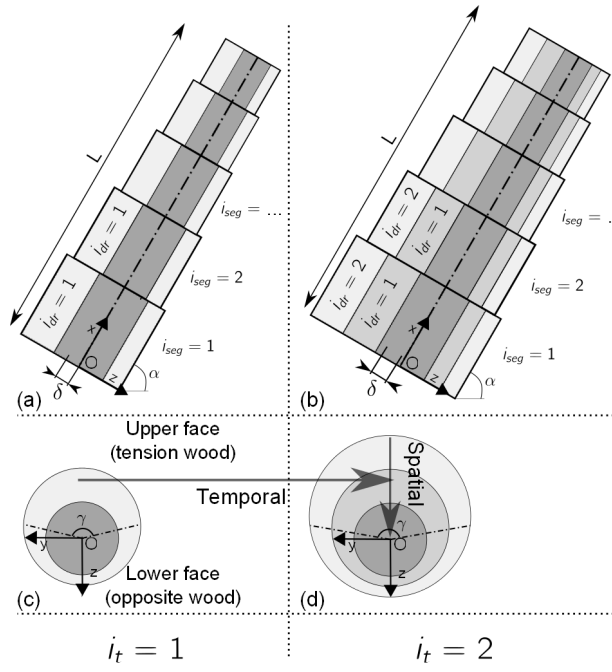


Fig. 1 Schematic representation of the modelling of the trunk in the longitudinal-radial plane (a, b) and radial-tangential plane (c, d) at two consecutive growth steps: $i_t = 1$ (a, c) and $i_t = 2$ (b, d)

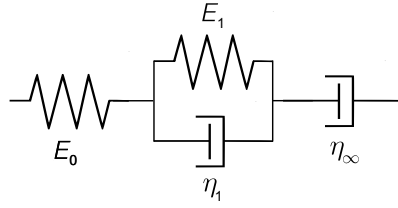


Fig. 2 Representation of a Burgers' rheological model

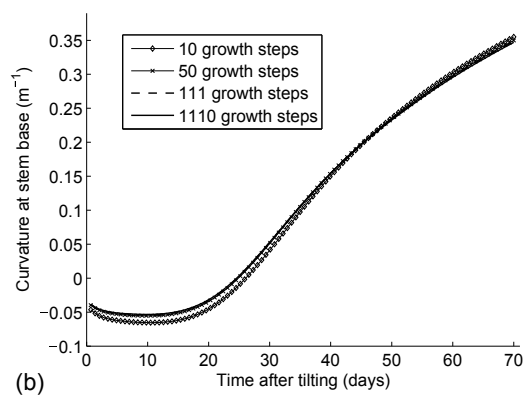
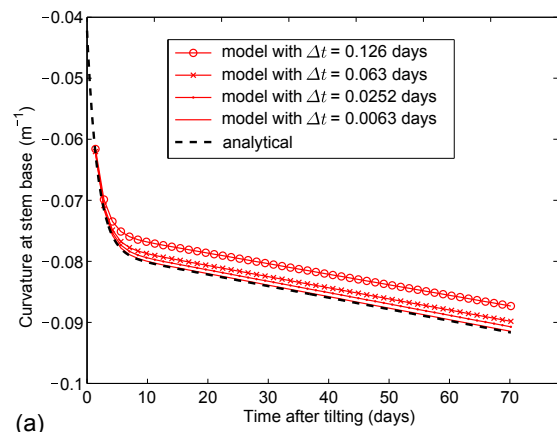


Fig. 3 Estimation of computational errors (a) Creep of a tilted wood beam under self-weight loading by numerical modeling and analytical calculation. (b) Temporal evolution of curvature at stem base for the gravitropic model with different growth increment sizes

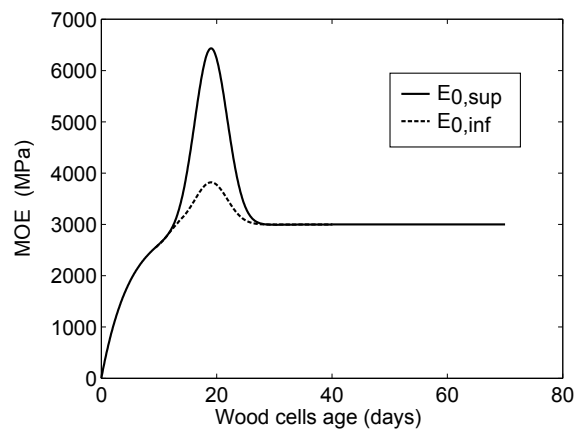


Fig. 4 MOE temporal variation with wood cell age used in the model for the upper side (TW) and lower side (OW)

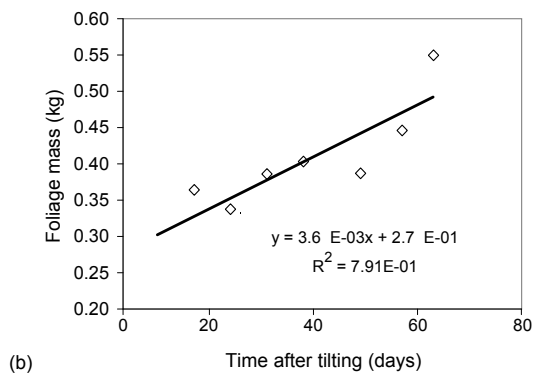
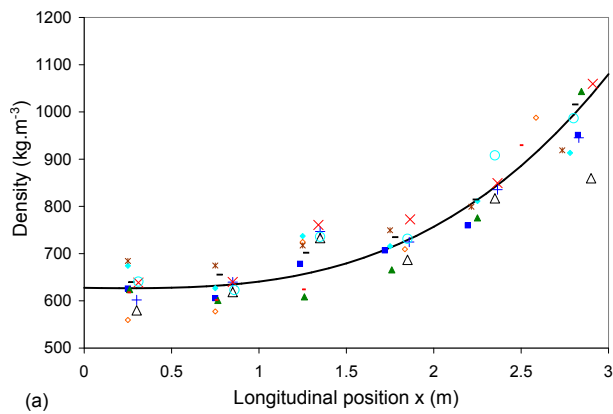


Fig. 5 (a) Variation in green wood density according to longitudinal position in the trunk for 2-year-old poplars. (b) Foliage mass for similar poplar trees felled at different dates along the season

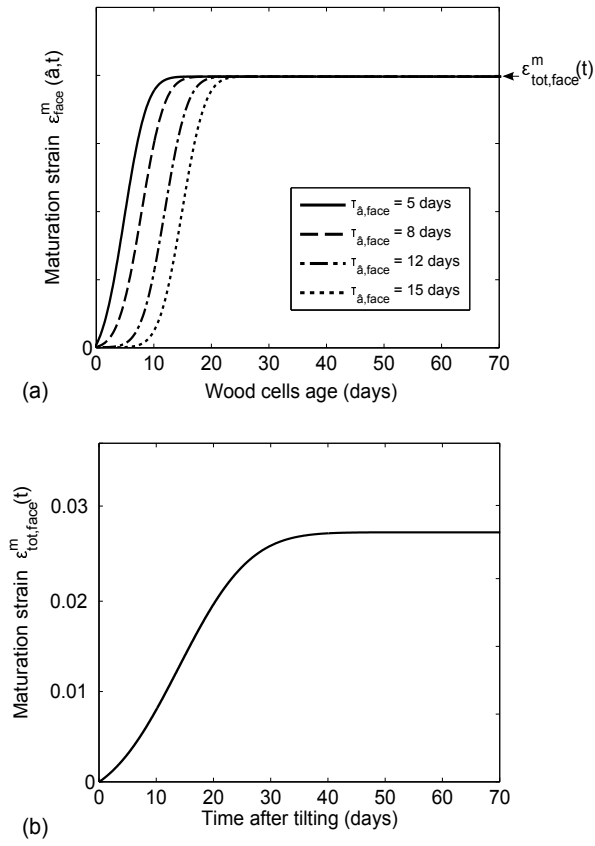


Fig. 6 (a) Normalized temporal variation in MS according to wood cell age for different values of $\tau_{\hat{a}, face}$. (b) Temporal variation in MS with time after tilting used for comparison between trees (values of table 2)

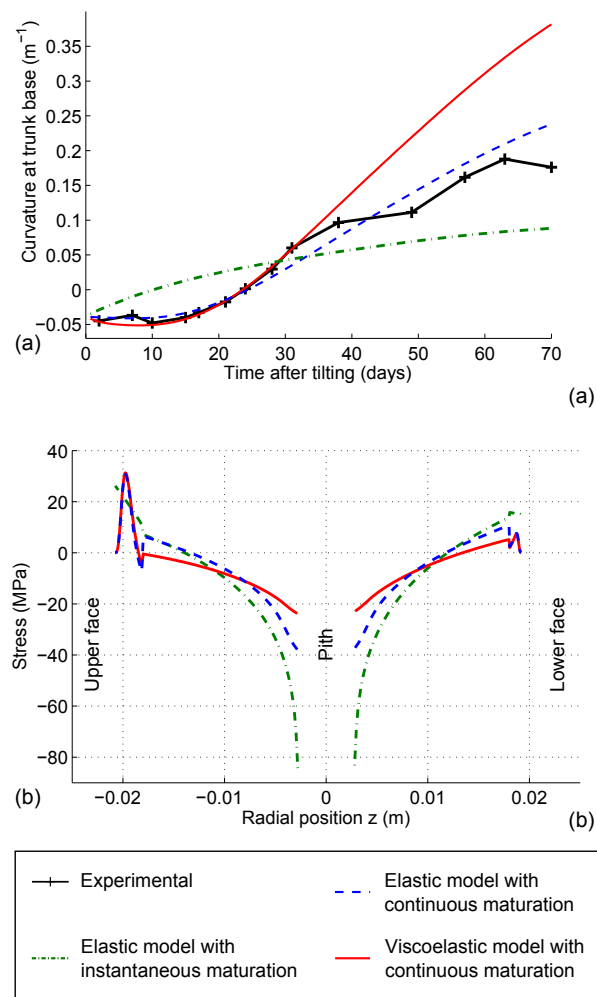


Fig. 7 Comparison of time variations in curvature at the trunk base (a) and stress profiles at the trunk base 28 days after tilting (b) between the experimental data of tree A and the model under different assumptions

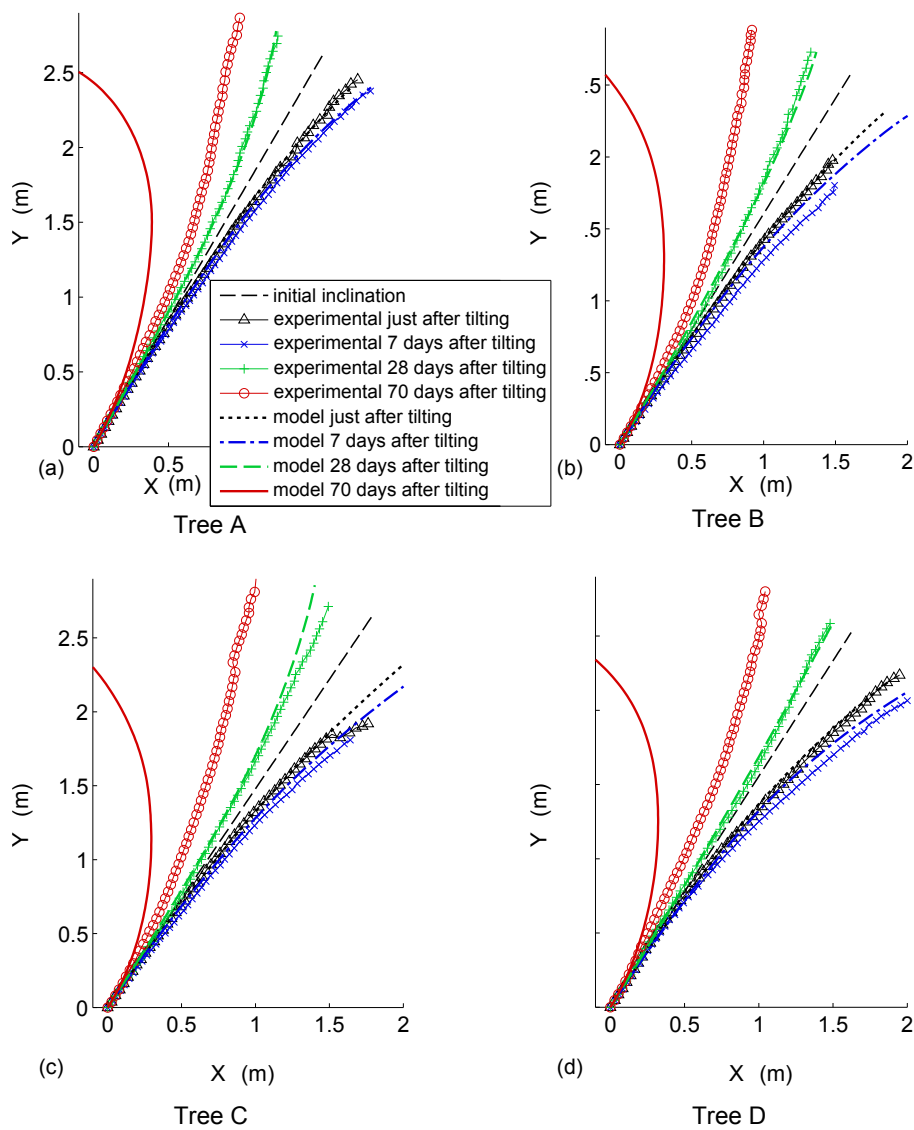


Fig. 8 Experimental and modelled shapes of different trees at different times along the season: just after tilting, 7 days, 28 days, and 70 days after tilting

Table 1 Diameter at the trunk base at the time of tilting and foliage mass 70 days after tilting for the 4 different trees studied

Tree	Diameter at trunk base at the time of tilting (mm)	Foliage mass 70 days after tilting (kg)
A	35.2	0.541
B	31.4	0.414
C	32.1	0.470
D	30.9	0.473

Table 2 Input parameters used for trees A, B, C and D for the viscoelastic model with progressive maturation

Parameters	Value and unit
Material properties (section 3.1)	
Burgers' parameter τ_1	38 hours
Burgers' parameter E_1	$E_1(\hat{a}) = 1.1 + 0.17\hat{a}$ (GPa)
Burgers' parameter $\frac{1}{\eta_\infty}$	$\frac{1}{\eta_\infty} = 6.75 \cdot 10^{-12} \exp(-9.4 \cdot 10^{-3}\hat{a})$ (Pa.jour) ⁻¹
Peak value of E_0 for OW	3800 MPa
Peak value of E_0 for TW	6500 MPa
Tree parameters (section 3.2 and 3.3)	
Length of the trunk L	Experimental measurement for each tree (m)
Radius of the trunk $r(x, t)$	Experimental measurement for each tree (m)
Initial tilt angle α	Experimental measurement for each tree (close to 35°)
Angular sector of TW γ	180°
Coefficient of eccentricity	0.4 m/m
Pith radius r_{pith}	2.65 mm
Wood density $\rho(x)$	Equation 13 (kg.m ⁻³)
Foliage mass linear repartition	Experimental measurement for each tree (kg.m ⁻¹)
MS parameters (section 3.4)	
Middle of MS temporal distribution of maturation $\tau_{\hat{a}, face}$	8 days
Width of the distribution of maturation $\delta_{\hat{a}, face}$	19 days
Middle of MS temporal distribution along the season $\tau_{t, face}$	14 days
Width of the distribution along the season $\delta_{t, face}$	59 days
Maximum value of MS on lower face $\varepsilon_{tot, inf}^m(t \mapsto +\infty)$	0.005 m/m
Maximum value of MS on upper face $\varepsilon_{tot, sup}^m(t \mapsto +\infty)$	0.027 m/m

Table 3 Results of the identification of MS parameters by fitting the temporal evolution of curvature at trunk base of tree C, for different values of $\tau_{\hat{a},face}$

Fixed parameter		Optimised parameters	
$\tau_{\hat{a},face}$ (days)	$\tau_{t,face}$ (days)	$\delta_{t,face}$ (days)	$\varepsilon_{tot,sup}^m(t \mapsto +\infty)$
5	21	66	0.044
8	14	59	0.027
12	1.6	47	0.014